Experimental investigation of the short-term creep recovery of hardened cement paste at micrometre length scale

Gan, Yidong; Vandamme, Matthieu; Chen, Yu; Schlangen, Erik; van Breugel, Klaas; Šavija, Branko

DOI
10.1016/j.cemconres.2021.106562

Publication date
2021

Document Version
Final published version

Published in
Cement and Concrete Research

Cement and Concrete Research 149 (2021) 106562

Contents lists available at ScienceDirect

Cement and Concrete Research

journal homepage: www.elsevier.com/locate/cemconres

Experimental investigation of the short-term creep recovery of hardened cement paste at micrometre length scale

Yidong Gan [a,*], Matthieu Vandamme [b], Yu Chen [a], Erik Schlangen [a], Klaas van Breugel [a], Branko Šavija [a]

[a] Microlab, Faculty of Civil Engineering and Geosciences, Delft University of Technology, Delft 2628 CN, the Netherlands
[b] Laboratoire Navier, Ecole des Ponts ParisTech, Univ Gustave Eiffel, CNRS, Marne-la-Vallée, France

ARTICLE INFO

Keywords:
Cement paste
Creep
Miniaturized cantilever beam
Nanoindenter

ABSTRACT

This paper presents an experimental investigation on the short-term creep recovery of cement paste at micrometre length scale. Micro-cantilever beams were fabricated and tested with 8 different loading series using the nanoindenter. It is found that cement pastes show high recovery ratios (>80%) even subjected to very high stress levels. Relatively lower recovery ratios and non-linear creep were also observed for w/c 0.4 samples under high stress levels. A good agreement is found between the results predicted using the linear superposition principle and the experimental results except for the measured non-linear creep in w/c 0.4 samples. It is suggested that the short-term creep recovery may be associated with the microscale stress redistribution or the reversible internal water movement. The observed non-linear creep under the highest stress level may be due to the higher density of microcracks generated during the loading stage, which may further promote the water transfer.

1. Introduction

Creep recovery of concrete is usually measured after the specimen that has been subjected to a sustained stress is unloaded [1]. Investigations on creep recovery of cementitious material are of importance in predicting the responses of concrete specimens under alternating stress [2] and also in elucidating the mechanism of creep [3,4]. Despite extensive research efforts [5–12,14], creep and creep recovery of concrete are still not completely understood. One of the encountered difficulties is the multiscale heterogeneous nature of cementitious materials [15–19]. It is generally recognized that creep of concrete mainly originates from the time-dependent behaviour of calcium silicate hydrate (C-S-H) at the nanoscale [7,18,20]. However, the interactions of C-S-H phases with other hydration products, pores, and pore water at the microscale or with aggregates at the mesoscale make it difficult to explain or predict the macroscopic creep behaviour of concrete [21–23].

In an effort to enhance the multiscale analysis of concrete creep, experimental techniques are needed to characterize the material over shorter length scales [22,24–26]. In this respect, many studies have employed the indentation technique to characterize the creep properties of cement paste at nano- or microscale [7,27–31]. It has been reported in these studies that the indentation testing method could largely reduce the characteristic time of the logarithmic creep, which often requires months or even years to be observed in macroscopic tests [7,25]. Therefore, the indentation technique is thought to be useful in characterising the long-term logarithmic type creep at the finer scale. On the other hand, a recently developed small-scale testing method on the micro-cantilever beam (MCB) [22,32,68] is found to enable the characterization of the short-term power-law type creep of cement paste at the micrometre length scale. Combining the indentation creep testing and small-scale testing methods may allow us to gain a complete description of creep behaviour at this scale [22,33]. However, compared to the large number of studies focused on the creep, relatively little is known about the creep recovery behaviour of cement paste at micrometre length scale. Recently, Liang and Wei [34] investigated the microscopic creep recovery of mature cement paste using microindentation technique for the first time. It is found that most of the measured microindentation creep deformations (around 65%) are non-recoverable. The authors [34] also suggested that the calculated recovery ratios in microindentation tests are comparable with that results obtained in the long-term compressive creep tests (0.25–0.31) [35]. This may indicate that the irrecoverable part of creep is associated with several irreversible long-term creep mechanisms, e.g. sliding,

* Corresponding author.
E-mail address: y.gan@tudelft.nl (Y. Gan).

https://doi.org/10.1016/j.cemconres.2021.106562
Received 1 December 2020; Received in revised form 30 May 2021; Accepted 31 July 2021
Available online 10 August 2021

dislocation, rearrangement or compaction of C-S-H [11,31]. Nevertheless, much uncertainty still exists about the recoverability of short-term creep mechanisms involved in the creep of cement paste at the micro-scale. Therefore, this study attempts to investigate the microscopic short-term recovery of cement paste using the MCB bending tests developed in [22]. This experimental approach was originally developed to characterize the short-term creep of cement paste at micrometre length scale and was extended here to consider the creep recovery behaviour of cement paste. It is hoped that the present research may gain more insights into the creep and creep recovery mechanisms of cement paste.

In this study, miniaturized samples (MCB) made of cement paste were fabricated using the method described in [22,32]. The nano-indenter was then utilized to perform creep and creep recovery tests on these MCBs. Several influencing parameters, such as w/c ratio, stress level and loading history, were investigated. The obtained creep and creep recovery results were first examined using the linear superposition principle. Afterwards, the comparisons with macroscopic and micro-indentation tests were conducted to gain insights of creep recovery behaviours. Moreover, several possible creep mechanisms were discussed to explain the observed creep recovery phenomenon.

2. Materials and methods

2.1. Materials and experimental procedure

2.1.1. Materials

Standard grade CEM I 42.5 N Portland cement and deionized water were used in this study. The Blaine fineness of cement is 2840 cm^2/g (provided by the manufacturer). The water/cement ratios of cement pastes were 0.3 and 0.4. Fresh cement paste was mixed following EN 196–3:2005 + A1:2008 (E) standard using a Hobart mixer and cast in plastic cylindrical moulds with 24 mm diameter and 39 mm height. To mitigate the influence of bleeding, the fresh paste was rotated at a speed of 2.5 rpm for 24 h at room temperature (26 °C). The samples were cured under sealed conditions at room temperature for 28 days. After demoulding, the hardened cement pastes were cut into 3 mm thick slices. The slices were then immersed in isopropanol to arrest the hydration [36].

2.1.2. Sample preparation

Micro-cantilever beams (MCBs) were prepared using a precision micro-dicing machine (MicroAce Series 3 Dicing Saw), which is generally used to cut semiconductor wafers. The first step is to obtain two smooth and parallel surfaces by grinding both the sides of cement paste slices using a Struers Labopol-5 thin sectioning machine. In the grinding process, two grinding discs of 135 μm and 35 μm were used in sequence. Once the thickness of 2.15 mm was reached, two perpendicular cutting directions with the same cutting space were applied on the samples using the micro-dicing machine. In this way, multiple rows of cantilever beams with a square cross section of 300 × 300 μm^2 were generated. The cutting depth, i.e. the cantilevered length, was approximately 1650 μm. The cutting process is schematically shown in Fig. 1. Several randomly selected beams were examined by using an Environmental Scanning Electron Microscope (ESEM) and X-ray computed tomography (XCT). An overall accuracy of the cross-sectional dimensions of ±1.5 μm can be reached with this fabrication process (Fig. 2). The X-ray source tube was set at 90 kV/100 μA during scanning resulting in a voxel resolution of 0.5 × 0.5 × 0.5 μm^3. After the segmentation of grey-value based CT images [37], the obtained porosities for MCBs with two w/c ratios are 4.39 ± 0.19% and 7.40 ± 0.43%, respectively. Note that due to the limitation of image resolution in XCT, pores smaller than 0.5 μm cannot be detected and are mixed within the segmented solid phases. Therefore, the porosity measured by XCT is much lower than the result of the mercury intrusion porosimetry (MIP) [38,39]. Besides, in both the ESEM and XCT images, no visible cracks have been found in MCBs. Before testing, precautions were also taken to minimize the carbonation of the samples by storing the beams in isopropanol.

2.2. MCB bending test

A KLA Nano indenter G200 equipped with a cylindrical wedge indenter tip (Fig. 3) is used to apply the bending load on the MCBs. Before testing, the angle and centre of the tip are calibrated by probing into the standard aluminium reference sample. The baseplate of MCB was fixed on a metal surface using cyanoacrylate adhesive. Afterwards, the angle of MCB is carefully adjusted under the in-situ microscope in the nanoindenter to ensure that the line load is applied perpendicularly to the beam longitudinal axis. The vertical line load was then applied by the nanoindenter on the free end of the beam. The experimental set-up is schematically shown in Fig. 4. For each tested beam, the coordinates of the loading position and the fixed end were recorded under the microscope to determine the loading length L. Prior to the tests, the samples were kept in the chamber for temperature equalization until the thermal drift rate is below 0.05 nm/s. All tests were conducted in a well-insulated chamber preventing any significant change of temperature and RH. The monitored average temperature and RH during the tests were 26.3 ± 0.4 °C and 34.2% ± 0.8%.

2.2.1. Flexural strength and elastic modulus

To determine the mechanical properties of MCBs, 30 beams for each w/c ratio were monotonically loaded to failure. The loading rate was 50 nm/s and the load-displacement responses of beams were recorded. The maximum load F_{max} and slope of load-displacement curve k during

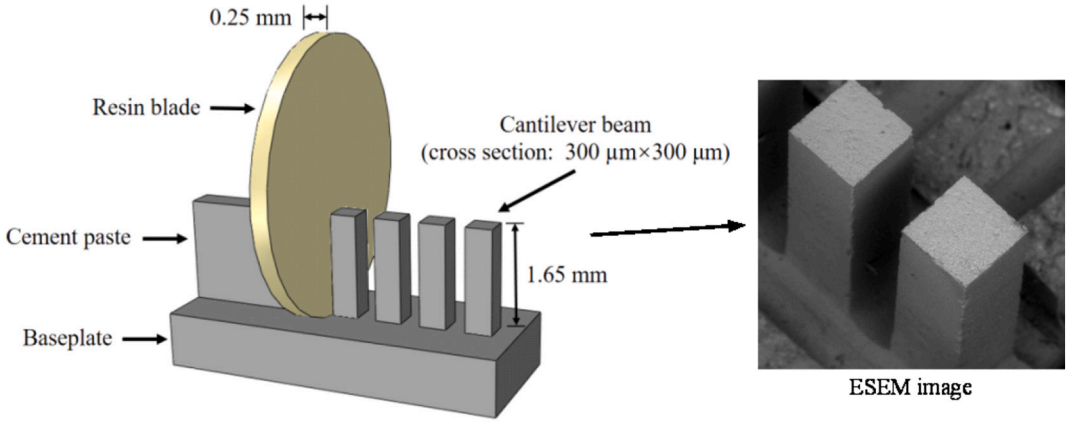

Fig. 1. Schematic diagram of sample preparation [22,32].

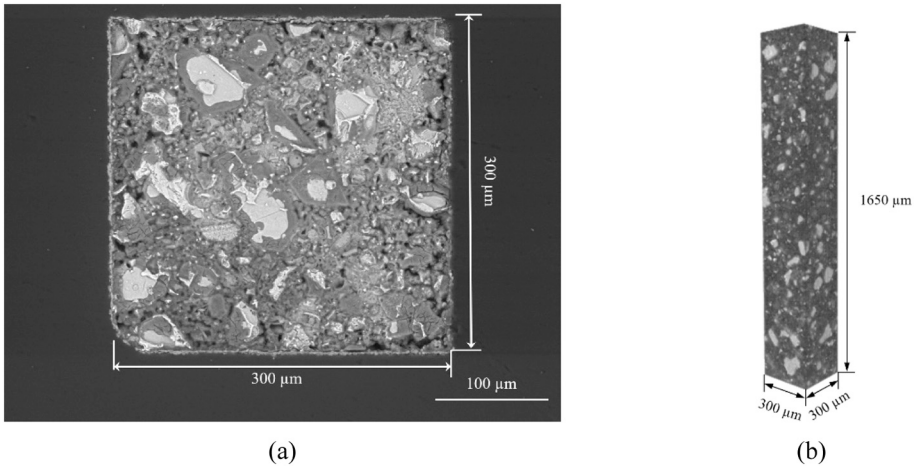

Fig. 2. (a) Backscattered electron image of the cross-sections of MCB with w/c 0.4; and (b) XCT image of MCB.

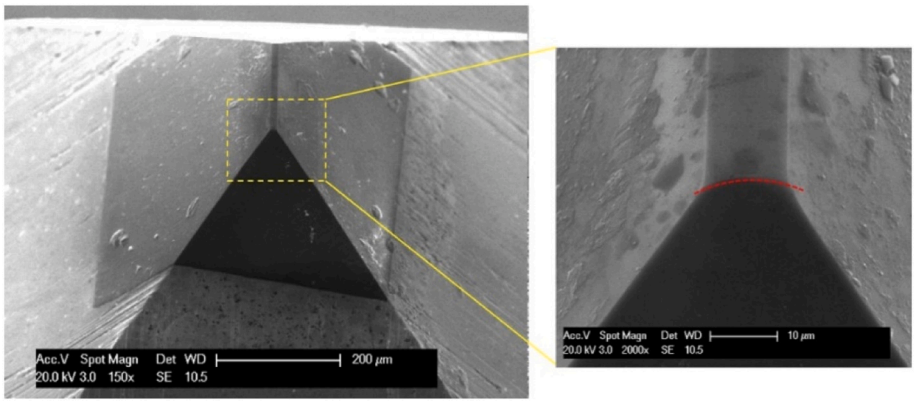

Fig. 3. Secondary electron image of the diamond cylindrical wedge tip with an enlarged view of the tip head [22].

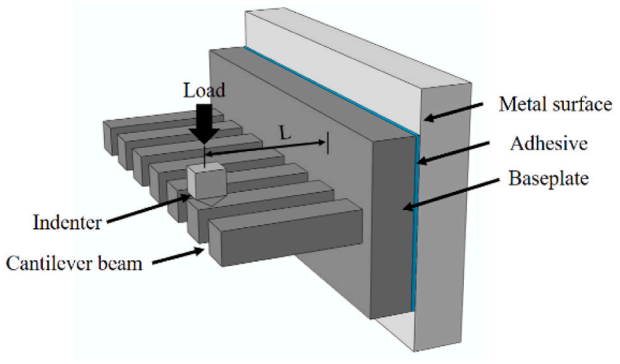

Fig. 4. Schematic diagram of test set-up [40].

loading are respectively used to determine the flexural strength f and loading modulus $E_{loading}$ according to the classical beam theory [22,32]:

$$f = \frac{F_{max} dh}{2I} \quad (1)$$

$$E_{loading} = \frac{kL^3}{3I} \quad (2)$$

where d is the measured distance between the load point and the fracture point, h is the side length of the square beam cross-section, and $I = h^4/12$ is the moment of inertia. For each w/c ratio, three beams were scanned by X-ray computed tomography. The measured loading modulus and flexural strength, as well as the calculated hydration degree based on XCT images [41] are presented in Table 1. As a demonstration, the MIP results of the cement pastes with similar material compositions, i.e. w/c ratio, age and curing condition, obtained in [39] are also presented in Table 1. As expected, the lower w/c ratio leads to higher mechanical properties mainly due to the decreased porosity [22,42]. The calculated flexural strengths are similar with the results reported in literature [22,32,43,44].

2.2.2. Creep and creep recovery test

The MCB bending test was used to characterize the creep and creep recovery properties of cement paste. The tests were carried out by the nanoindenter using load control. The measurement frequency of each test is 5 Hz. Before each MCB bending test, the beam was preloaded to 60% of constant load (which will be applied in the following creep test) in 5 s and then unloaded completely also in 5 s. This procedure aims to mitigate the possible plasticity in the experimental set-up and at the same time to reduce possible initial damage to the sample and improve

Table 1
Porosities and mechanical properties of MCBs (in total 66 beams tested).

w/c ratio	Porosity by MIP (%) [39]	Hydration degree (%)	$E_{loading}$ (GPa)	f (MPa)
0.3	17	75.35 ± 3.18	20.66 ± 1.49	29.24 ± 2.61
0.4	23	80.57 ± 4.69	15.14 ± 1.61	22.65 ± 2.64

the repeatability of the results. In the creep and creep recovery tests, the load is first increased to the prescribed maximum force in a short period (e.g. 5 s). The load is then held for a certain period (e.g. 180 s) to measure the change of deformation as shown in Fig. 5(a). During the unloading stage, the load is decreased to 1% of maximum force in 5 s. This is followed by the second holding stage, where the small load (1% of maximum force) is sustained. The original purpose of this re-holding stage programmed in the Nano indenter G200 is to assess the thermal drift rate at the end of test. However, the measured drift rate will be affected by the creep recovery of cement paste due to its viscoelastic nature. Herein, the second holding stage with another time period (e.g. 600 s) is used to estimate the creep recovery by recording the change of displacement at this stage. The applied small load is to guarantee that the indenter tip remains in contact with the sample's surface. This is somewhat different from the creep recovery measurement in the macroscopic test, where the load is completely removed.

Due to the extremely thin cross-section of MCB and the short testing duration of 790 s with a constant RH, additional time-dependent deformations resulting from the autogenous shrinkage, drying shrinkage and drying creep, etc. can be neglected. The creep strain $\varepsilon_{bc}(t)$ at the upper fibre of the fixed end of beam can be calculated as:

$$\varepsilon_{bc}(t) = \frac{3\delta_{bc}(t)h}{2L^2} \tag{3}$$

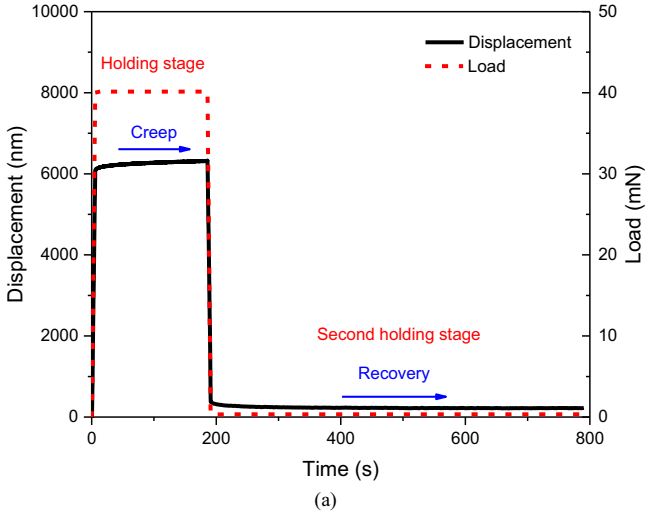

(a)

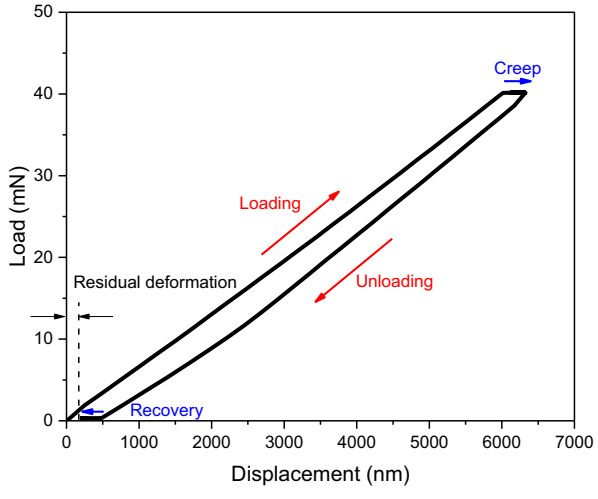

(b)

Fig. 5. Typical measured curves using the testing protocol.

Note that the creep strain generated in the loading stage cannot be neglected even subjected to the short loading duration (5 s) [33,40]. This part of creep strain will be calculated based on the proposed analytical equations in next section.

In conventional nanoindentation tests, plasticity is often generated during the loading stage because of the local high stress generated under the tip [45]. In this study, some residual deformation d_{res} is observed at the end of test, as can be seen in Fig. 5(b). The residual deformation after excluding the displacement caused by the re-holding load, which is calculated using the loading modulus, is only 2%–4% of the displacement at the end of loading stage. By calculating the loading and unloading slope in the range between 40% and 60% of maximum force, the corresponding moduli, i.e. $E_{loading}$ and $E_{unloading}$, can be obtained according to Eq. (2). The determined $E_{loading}$ and $E_{unloading}$ for w/c 0.3 samples are 20.25 ± 1.75 MPa and 21.04 ± 1.81 MPa, respectively. For w/c 0.4 samples, the calculated loading and unloading moduli are 15.06 ± 1.52 MPa and 15.67 ± 1.60 MPa, respectively. Note that there will be a small difference of slope determined from other loading ranges. Fig. 6 shows a comparison between the loading and unloading modulus. The calculated loading modulus is around 3% lower than the unloading modulus indicating that the plastic deformation generated during the loading stage accounts for a major portion of the residual deformation. The plastic deformation may include the accumulated damage inside the beam, possible indentation depth into the beam surface, as well as other non-recoverable deformations inherent to the experimental set-up. However, no plastic deformation is expected in the holding stage and the unloading stage. In addition, a small portion of the residual deformation could also be attributed to the ongoing recoverable creep and possible non-recoverable creep.

The influences of different loading procedures on the creep and creep recovery of cement paste at micrometre length scale were investigated in this study. Table 2 presents 8 test series of the MCB bending tests. In each test series, more than 15 MCBs were tested and the measured creep and recovery displacements were averaged as illustrated in Fig. 7. It should be mentioned that the directions of creep and recovery are opposite though they are both plotted with the positive sign. The total test duration is limited within 800 s due to the technical restriction of the nanoindenter. In test series 1–6, three different loading levels were applied for each w/c ratio, while the loading duration is kept the same with the unloading duration (5 s) and all the holding and re-holding durations are constant amounting to 180 s and 600 s, respectively. In test series 7, the holding duration is increased to 300 s and the second holding duration of 300 s is used. The loading duration up to 50 s was

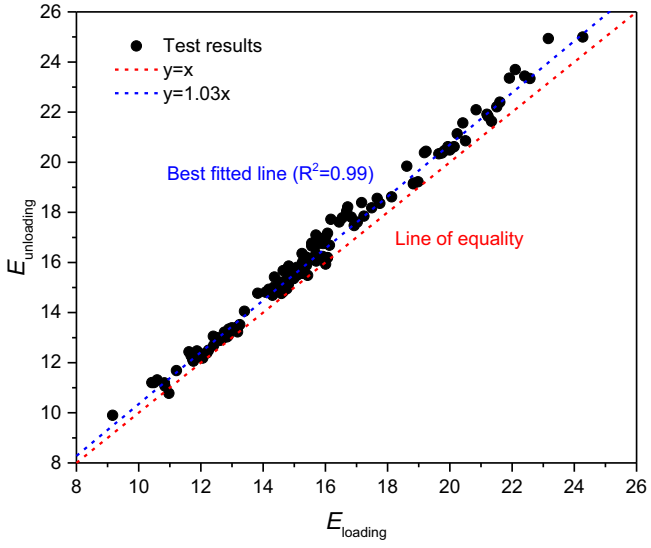

Fig. 6. Comparison of measured loading and unloading modulus.

Table 2
Summary of the loading procedures for MCB bending tests.

Test series	w/c	Loading duration (s)	Holding load (mN)	Stress level	Holding duration (s)	Second holding load (mN)	Second holding duration (s)
1	0.3	5	40	46%	180	0.4	600
2	0.3	5	60	69%	180	0.6	600
3	0.3	5	80	92%	180	0.8	600
4	0.4	5	20	30%	180	0.2	600
5	0.4	5	40	59%	180	0.4	600
6	0.4	5	60	88%	180	0.6	600
7	0.4	5	40	59%	300	0.4	300
8	0.4	50	40	59%	180	0.4	300

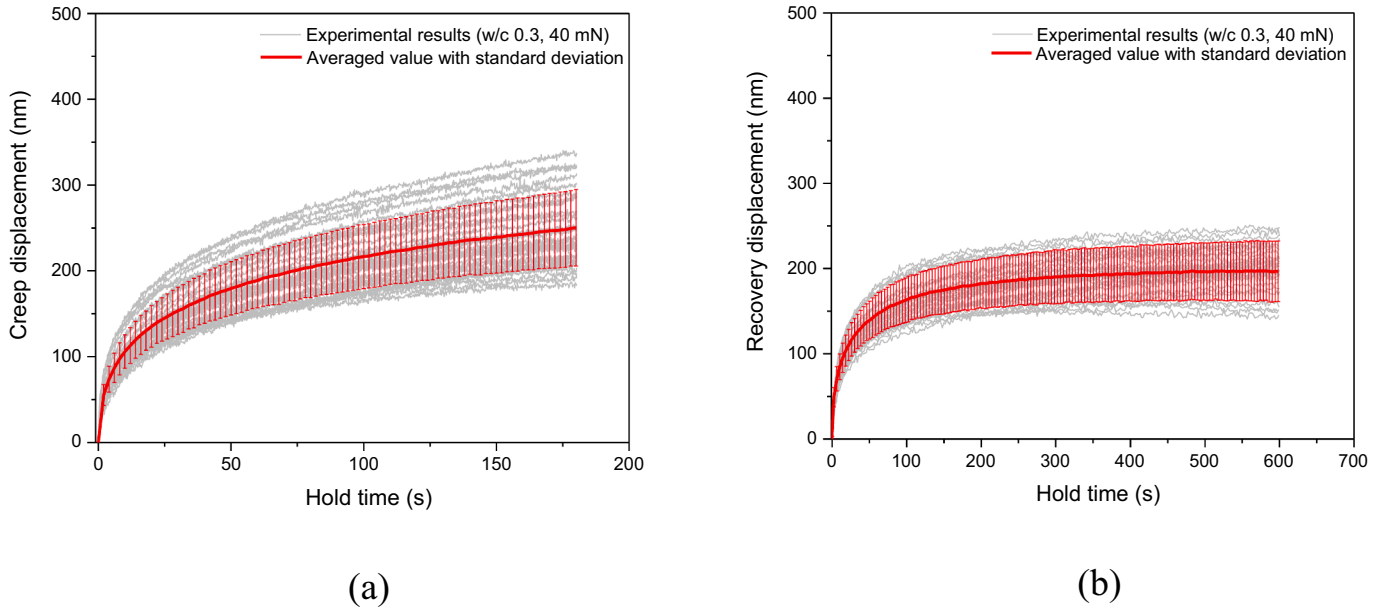

Fig. 7. The measured creep and creep recovery displacement evolution curves during the holding stages for w/c 0.3 samples at the loading level of 40 mN.

investigated in test series 8.

In the course of experiments using the nanoindenter, the thermal drift may also play a role. Therefore, 15 MCBs made of glass were fabricated and loaded using the same loading procedure in order to evaluate the drift rate and validate the experimental method. The measured displacements for glass MCBs at the holding and re-holding stages are compared with the results of cement paste MCBs in Fig. 8. Generally, the glass is expected to exhibit no creep at room temperature [46]. Therefore, any measured time-dependent deformation for glass tests should be attributed to the inherent drift of the equipment or the test set-up. It can be seen in Fig. 8 that the measured time-dependent deformation for glass beams is very small compared to that of the

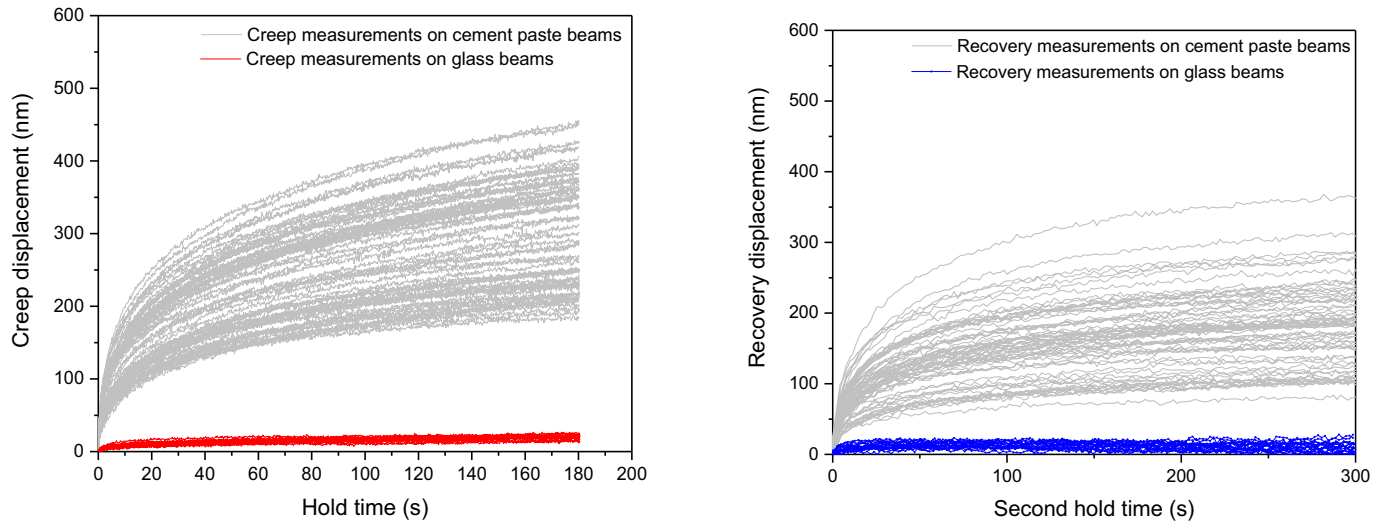

Fig. 8. The comparisons of creep and creep recovery during the holding stages between cement paste beams and glass beams.

cement paste beams. The thermal drift rate may vary slightly between each test. For simplicity, the measured drift rates of the glass beams, including holding and re-holding stages, were assumed to be constant and the averaged value (including positive and negative drift rate) is 0.026 nm/s ± 0.009 nm/s. Therefore, the total drift for the testing duration of 790 s is around 20.54 nm. The obtained drift rate will be adopted in the analytical model in the following section.

2.2.3. Analytical evaluation of visco-elastic-plastic deformation

The measured total displacement of MCB δ_{total} during the whole testing duration is assumed to consist of four main parts: instantaneous elastic deformation δ_e (reversible), plastic deformation δ_p (irreversible), viscoelastic deformation δ_v (reversible) and thermal drift δ_d (irreversible). The recoverable elastic deformation is linearly dependent on the magnitude of the load and can easily be determined based on the Hooke's law. The magnitude of plastic displacement during the loading stage is here assumed to increase linearly with the load for the sake of simplicity. It is known that the viscoelastic response is a function of the entire loading history [33]. The cement paste at the micrometre length scale is initially considered as a linear viscoelastic solid. For small deformations, the Boltzmann superposition principle (BSP) can be applied to evaluate its time-dependent response subjected to any arbitrary load. In the region of linear viscoelasticity, the BSP states that the response of a material to a given load is independent of responses of the material to any load already acting on the material [47]. It means that each increment of load exerts an independent and additive contribution to the total viscoelastic deformation. Besides, the deformation of a specimen is proportional to the applied stress when all deformations are compared at equivalent times. Based on these assumptions, this principle permits the calculation of viscoelastic deformation of material subjected to arbitrary stress history. The basic creep compliance evolution of cement paste can generally be constructed from combinations of rheological models, i.e. linear springs and viscous dashpots. Alternatively, the creep compliance function can also be determined through experimental data. In this study, the power-law function mentioned is used [22,33,48]. The specific basic creep compliance curve $C(t,t_0)$ can be represented as follows:

$$C(t,t_0) = \alpha\left(\frac{t-t_0}{t_1}\right)^{\beta} \tag{4}$$

where t_0 is the time at the beginning the holding stage; $t - t_0$ is the time elapsed under constant loading; t_1 is the reference time unit, i.e. 1 s. α and β are two fitting parameters, where the inverse of α corresponds to the so-called creep modulus [33]. The formulation of the BSP for a multistep creep strain ε_{creep} of cement paste under isothermal conditions reads:

$$\varepsilon_{creep}(\sigma,t) = \sum_{i=1}^{n}[\sigma(t_i)-\sigma(t_{i-1})]\left[\alpha\left(\frac{t-t_{i-1}}{t_1}\right)^{\beta}\right] \tag{5}$$

where $\sigma(t_i) - \sigma(t_{i-1})$ is the actual stress increment at time interval $(t_i - t_{i-1})$. The time interval used in this study is 0.1 s. In addition, the thermal drift rate is assumed here to remain constant during the creep and recovery test. Therefore, by converting the viscoelastic strain to viscoelastic displacement using Eq. (3), the total displacement evolution can be written as:

$$\delta_{total}(t) = \delta_e + \delta_v + \delta_p + \delta_d = \frac{2L^2}{3h}\left[\frac{\sigma(t)}{E_{int}} + \varepsilon_{creep}(\sigma,t)\right] + \sigma_{loading}(t)\frac{d_p}{\sigma_{max}} + \gamma_{drift}t \tag{6}$$

where E_{int} is the fitted intrinsic elastic modulus, $\sigma_{loading}(t)$ is the stress applied to the sample up to time t, d_p is the non-recoverable plastic displacement generated during the loading stage, σ_{max} is the maximum stress, γ_{drift} is the drift rate (0.026 nm/s) determined from tests of glass beams. It should be mentioned that since the current focus is to examine the validity of BSP, we performed simplified optimization processes for determining the two creep function parameters (α and β), which is similar to the approach used in [33,49]. Only three search intervals for each parameter were defined and used to iteratively find the minimal difference between the predicted and measured creep compliances [33]. To quantify the difference between the predicted and measured creep curves, the square root of sum of squares error value ε_{error} at each time point is calculated. The optimization processes were performed on two test series, i.e. test series 2 (w/c 0.3) and test series 5 (w/c 0.4). These two series with moderate stress levels were selected in order to minimize the effects of other time-dependent deformation as well as non-linear creep. Afterwards, the identified creep parameters were directly applied to other test series. The rest of parameters used in Eq. (6) are fitted separately using different parts of the load-displacement and time-displacement curves. It is worth to noting that these parameters may slightly differ for each individual sample due to the heterogeneous nature of cement paste.

3. Results

3.1. Identification of visco-elastic-plastic parameters

An example of the predicted displacement evolution of one MCB based on Eq. (6) is shown in Fig. 9. In general, the predicted displacement-time curve agrees well with the experimental curve.

The identified parameters for all test series are present in Table 3. For w/c 0.3 samples in test series 2, the two parameters fitted best for the measured average creep compliance function, i.e. α and β, are 1.17 ± 0.12 × 10^{-3}/GPa and 0.203 ± 0.012, respectively. While for the w/c 0.4 samples, the average values with their standard derivations of two parameters were determined as 1.47 ± 0.27 × 10^{-3}/GPa and 0.203 ± 0.011. The creep parameters identified from the test series 2 and 5 were directly used in other test series with the same w/c ratio. It can be seen that the obtained average E_{int} for w/c 0.3 and 0.4 sample are both slightly larger than the corresponding loading and unloading moduli. Based on the holding and unloading curves, the creep parameters and intrinsic elastic modulus can be determined. By deducting the thermal drift, elastic deformation (at 1% maximum load) and remaining viscoelastic deformation (to reach 100% recovery) from the total measured residual deformation at the end of test, the plastic deformation can be determined. Note that no plastic displacement is assumed at the holding stage.

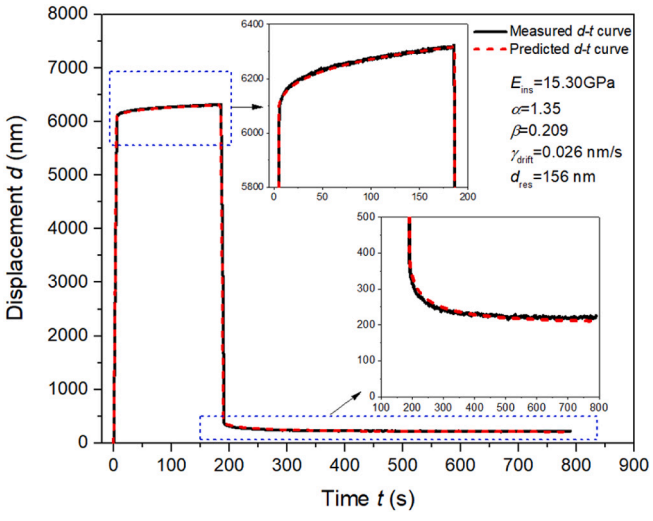

Fig. 9. A typical comparison between the measured and predicted displacement-time curve for one w/c 0.4 sample from test series 5.

Table 3
Summary of fitting parameters for 8 test series.

Test series	w/c	σ_{max} (MPa)	α (10^{-3}·GPa^{-1})	β	E_{int} (GPa)	d_p (nm)	γ_{drift} (nm/s)	ε_{error} (nm)
1	0.3	13.32 ± 0.02	1.17	0.203	21.87 ± 1.41	205 ± 131	0.026	9.63 ± 4.57
2	0.3	20.01 ± 0.03	1.17	0.203	21.67 ± 1.76	219 ± 105	0.026	3.25 ± 1.75
3	0.3	26.73 ± 0.05	1.17	0.203	21.41 ± 1.56	280 ± 143	0.026	4.25 ± 4.04
4	0.4	6.68 ± 0.03	1.47	0.203	16.22 ± 1.17	226 ± 73	0.026	2.74 ± 2.12
5	0.4	13.34 ± 0.01	1.47	0.203	16.34 ± 1.62	260 ± 95	0.026	2.96 ± 1.56
6	0.4	19.91 ± 0.02	1.47	0.203	15.88 ± 1.77	369 ± 124	0.026	14.99 ± 6.59
7	0.4	13.27 ± 0.02	1.47	0.203	16.53 ± 1.21	271 ± 108	0.026	3.12 ± 1.62
8	0.4	13.29 ± 0.03	1.47	0.203	15.95 ± 1.50	332 ± 103	0.026	10.93 ± 6.34

3.2. Creep strain evolution

Based on previous analytical equations and identified parameters, it is now possible to estimate the development of the creep strain (visco-elastic strain) during the whole test including loading, holding and unloading stages. As a demonstration, the calculated viscoelastic strain evolution curve for a w/c 0.4 sample under the loading level of 40 mN is shown in Fig. 10. In this case, the viscoelastic strain generated during the loading stage (5 s) is almost 67.7% of the viscoelastic strain developing during the subsequent holding stage (180 s). In addition, the magnitude of viscoelastic strain generated during the unloading stage (5 s) is around 24.46 με, which is very close to the viscoelastic strain at the loading stage (25.05 με). The creep strain evolution defined in this study is mainly composed of two parts, i.e. the calculated viscoelastic strain at the loading stage and the measured time-dependent strain at the holding stage. For the case of test series 8, where 50 s loading duration was used, the calculated creep strain during the loading stage amounts to approximately 166.7% of the additional creep strain developing during the subsequent 180 s of constant loading.

The creep strain evolutions of MCBs were then divided by the applied maximum stresses, which are determined using Eq. (1), to obtain the creep compliance curves. Fig. 11 shows the creep compliance curves for two w/c ratios samples under different loading levels. For w/c 0.3 samples, the overall differences of creep compliances are very small. It confirms that the cement pastes in the short-term behave in a linear viscoelastic manner at the micrometre length scale. For the w/c 0.4, the creep compliances of the first two loading levels, i.e. 20 mN and 40 mN, almost overlap, while for the highest loading level (60 mN), the creep compliance is larger.

Fig. 12 compares the creep compliance curves of w/c 0.4 samples

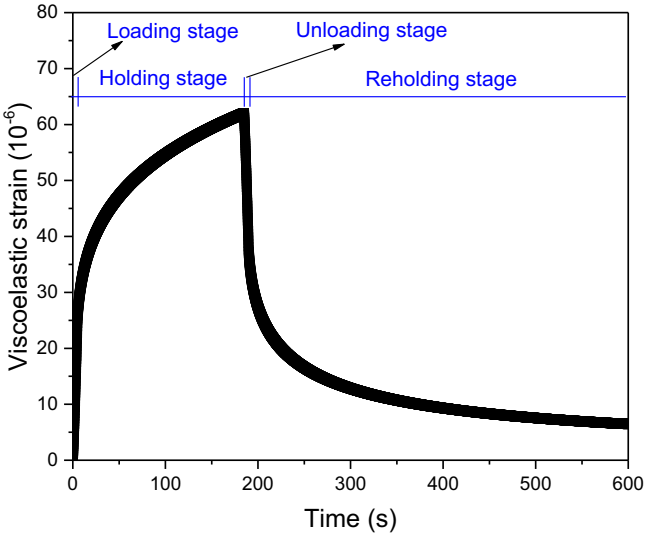

Fig. 10. The calculated evolution of viscoelastic strain of w/c 0.4 sample under the loading level of 40 mN.

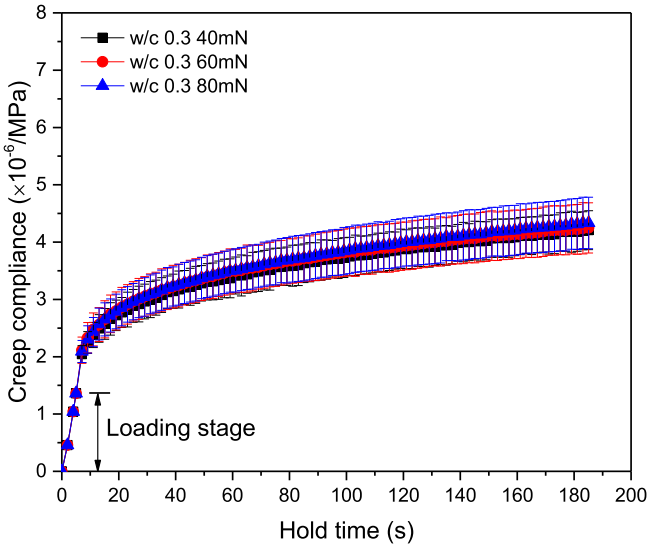

(a)

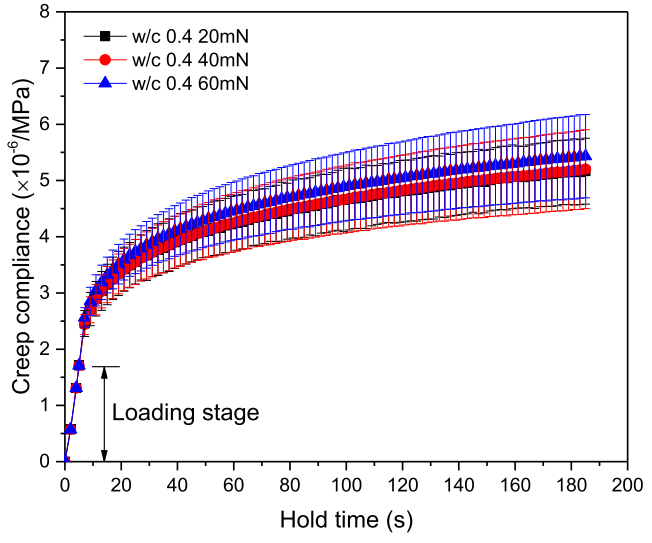

(b)

Fig. 11. The average creep compliances with scatter bars for (a) w/c 0.3 samples, and (b) w/c 0.4 samples.

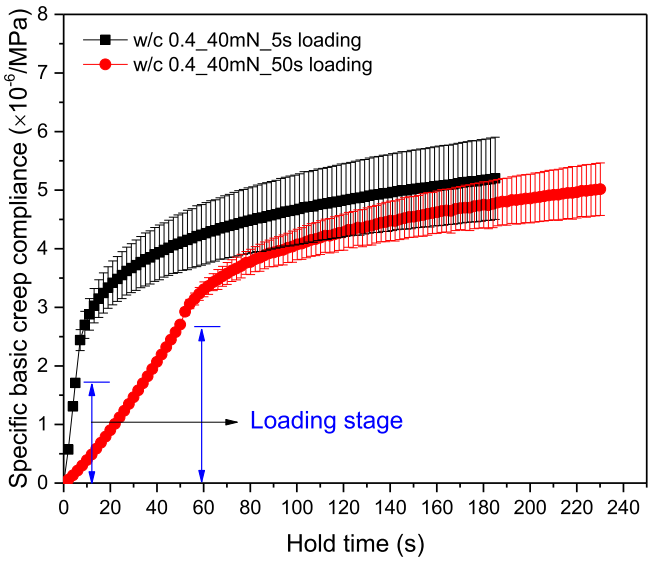

Fig. 12. The comparison of creep compliance evolutions for two different loading durations.

with different loading durations. In the loading stage, the calculated creep compliance is increased in slower loading procedure with the same holding load. Moreover, less creep compliance is generated during the holding stage when the longer loading duration is used. It also needs to be noted that the viscoelastic deformation generated during the loading stage will affect the determination of elastic modulus [40].

The derivatives of the data from Fig. 11 were calculated as the rates of creep compliance at the holding stage. When the rate of creep compliance versus time is plotted on a log-log scale, a single straight line can be found for each sample, see Fig. 13. The curves for different samples have similar slopes in the log-log scale suggesting a constant exponent in the creep compliance function [22,33].

3.3. Creep recovery measured at the second holding stage

The change of displacement measured over the second holding stage is considered as the main part of the creep recovery. The measured creep recovery for samples subjected to different loading levels is plotted as a logarithmic function of time in Fig. 14. Similar observations with respect

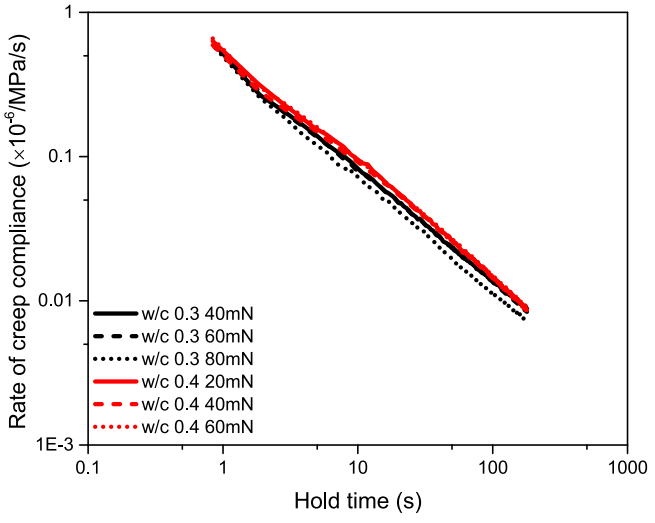

Fig. 13. The calculated average rate of creep compliance during the holding stage.

to the shape of creep recovery curve were reported in [50], where a short-term transition was found in the time range from 0.2 s to 10 s for macroscopic four-point bending tests on hardened cement paste. In general, the creep recovery displacement increases with the loading levels as more recoverable creep deformation is generated during the holding stage. Likewise, when the loading duration or holding duration is increased, more creep recovery will also be measured in the second loading stage, as shown in Fig. 15.

It has been reported in several studies [34,51,52] that the rate of creep recovery shows a rapid devolvement followed by a slow one. Herein, the averaged creep recovery rates, which have been normalized by the applied stresses at the first holding stage, are plotted against time on a log-log scale in Fig. 16. Generally, the rate of creep recovery gradually decreases with time, but there are clearly two different attenuation speeds observed in each sample for both w/c ratios. As a result, two distinct stages are recognized in Fig. 16 and it is found that the corresponding transition point always lies in the time range of 15 s–20 s. Similar transition point has also been observed for other test series. The attenuation speed for the creep recovery rate in the first stage is slower than that of the second stage. In addition, the magnitude of creep recovery rate seems to be proportional to the stress.

The initial recovery rates per unit stress at the beginning of the second holding stage for both w/c ratios are presented in Fig. 17. It can be seen that the initial recovery rates for w/c 0.4 at low stress levels are higher than that of samples with w/c 0.3. It is interesting to note that the initial recovery rate is around 23% larger for w/c 0.4 than for w/c 0.3, while the creep compliance for w/c w 0.4 is also around 22% larger than for w/c 0.3 (in Fig. 11). For samples with w/c 0.3, the initial recovery rates per unit stress are almost independent of the applied stress. However, for w/c 0.4 samples, when the stress is around 20 MPa, a notable drop was observed.

3.4. Creep recovery ratio

The creep recovery ratio is here defined as the ratio between the total creep recovery displacement and the total creep displacement. Note that the creep and recovery displacement at holding stages were experimentally measured, while the displacements at the loading and unloading stages were calculated based on Eq. (6). The average creep recovery ratios for eight test series are shown in Fig. 18. The second holding duration is 300 s in both test series 7 and 8, while 600 s is used in the other test series. Since a large portion of the creep recovery has been completed within 300 s (as shown in Fig. 7), the two different holding durations are expected to exhibit negligible influence on the recovery ratio. It can be seen from Fig. 18 that most recovery ratios reach at around 70%–90%. It also appears that the recovery ratios are independent of the w/c ratio for the same loading level. For w/c 0.3 samples, the recovery ratio is not largely affected by the change of the applied (constant) load. The recovery ratio only drops 3.9% from the lowest constant load to the highest constant load. However, for w/c 0.4 samples, a notable drop in recovery ratio (around 11.5%) is observed for the samples under the highest constant load (60 mN), indicating some irrecoverable creep was generated during the holding stage. For test series 7, where a longer holding duration (300 s) was used, more creep displacement would be expected and the recovery ratio would be lower compared to those of tests with 180 s holding durations. As for the test series 8, where 50 s loading duration was used, the calculated recovery ratio is around 84.7%, which is similar to the results of other w/c 0.4 test series.

3.5. Comparisons between experimental results and analytical predictions

The identified creep parameters with the real loading history and a constant drift rate (0.026 nm/s) were used in the analytical Eq. (6) to predict the creep recovery curves under different loading levels, as shown in Fig. 19. It can be seen that the overall differences between the

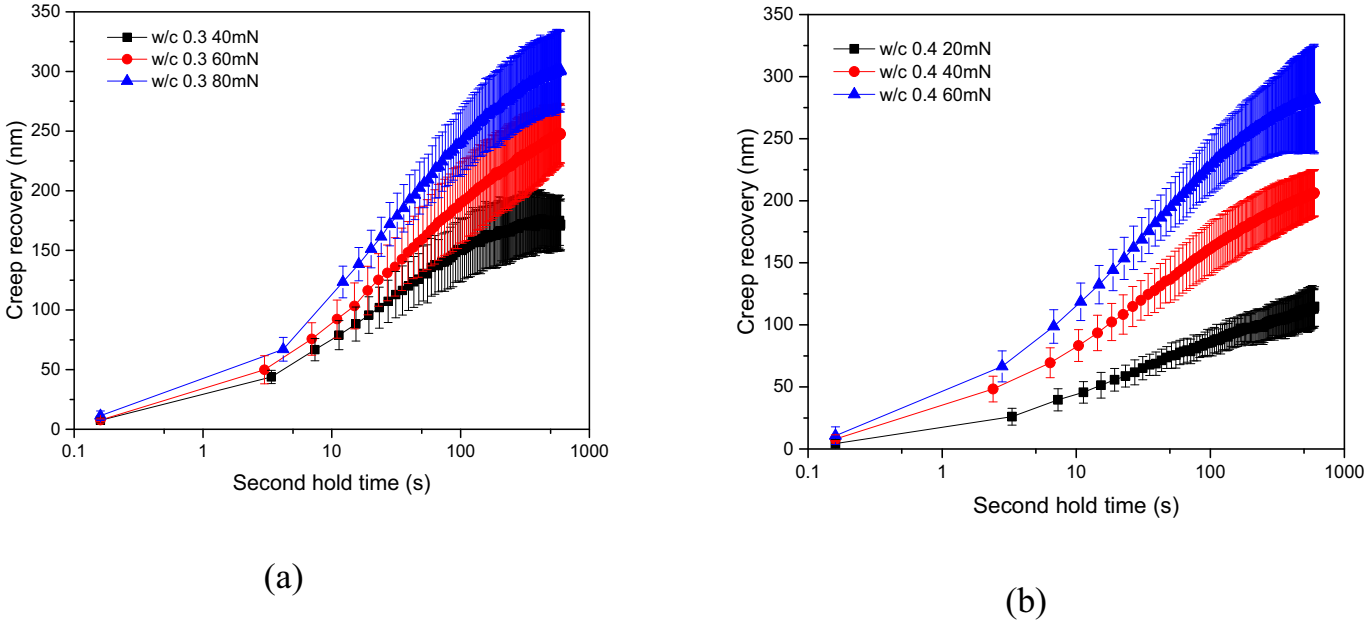

Fig. 14. The measured creep recovery evolution curves at the second holding stage for (a) w/c 0.3 and (b) w/c 0.4 samples.

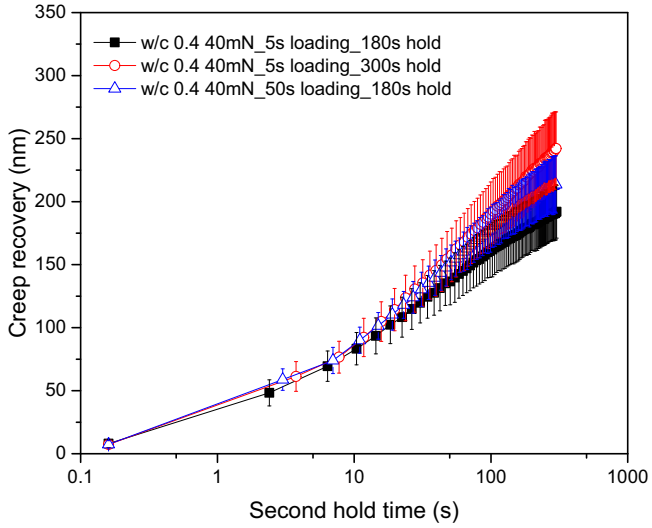

Fig. 15. The measured creep recovery at the second holding stage for different loading histories.

predicted and measured average creep recovery curves are small. In Table 3, the ε_{error} calculated for w/c 0.3 with the applied load of 40 mN is 9.63 ± 4.57 nm, while for the other two loading levels the average error values are only 3.25 ± 1.75 nm and 4.25 ± 4.04 nm. This large prediction error for w/c 0.3 samples under the lowest loading level may be attributed to the assumed constant drift rate, which will be explained later. Exceptions have also been observed for w/c 0.4 samples under the highest loading level, where the measured creep recovery is lower than the predicted value. It suggests that the linear viscoelastic principle may be not applicable anymore for w/c 0.4 cement paste with the stress amounting to around 20 MPa (corresponding to the force of 60 mN and around 88% of strength).

The predicted evolution of creep compliance with two different loading durations, i.e. 5 s and 50 s, are presented in Fig. 20(a). In general, the predicted creep compliance curves of cement paste (w/c 0.4) during the holding stage agree well with the experimental results. However, the analytical equation shows relatively limited success in predicting the test series with the loading duration of 50 s, as indicated by the calculated ε_{error} in Table 3. This is probably attributed to the assumed constant drift rate. The analytical equation was also utilized to examine whether the adopted re-holding protocol with 1% of maximum load may bias the kinetics of creep recovery development. As shown in Fig. 20(b), negligible influence on the kinetic of creep recovery can be observed confirming the validity of the current testing protocol.

The analytical equation was then used to predict the creep recovery ratios for different w/c ratios and applied stress levels. Moreover, the effect of drift rate, which is inherent to the nanoindenter measurement, on the measured creep recovery ratios was also assessed. The predicted and measured recovery ratios are shown in Fig. 21. When the drift rate is set to zero, the predicted recovery ratio is independent of the applied stress and is calculated as around 90.1%, which is close to most of the experimentally measured ratios. However, the assumed positive drift rate will lower the predicted recovery ratio and make it even closer to the experimental results. When the drift rate is assumed to be 0.026 nm/s, there is an increasing trend for the predicted recovery ratio with the increasing stress. This spurious dependency on stress magnitude is due to the decreasing proportion of drift in total deformation. The drift also accounts for a higher portion of the total deformation for lower w/c ratio samples as their total deformations are relatively small. Therefore, one should always be careful with interpreting the time-dependent deformation measured by the nanoindenter as they may be biased by the drift rate, which is not an intrinsic material behaviour. Besides, there is no guarantee that the thermal drift will remain constant during the tests. However, as long as the total deformation is large enough and the total duration short enough, the effect of drift can be neglected.

Overall, the time-dependent deformation of the cement paste at micrometre length scale can be appropriately described based on the linear superposition principle, except for the case of test series 6 where non-linear creep was observed. However, it should be mentioned that the maximum stress applicable for linear viscoelasticity of cement paste at micrometre length scale is much higher than the values reported in most macroscopic flexural or tensile creep tests. For w/c 0.3 samples, the applied stresses even reach to around 92% of the flexural strength and the samples almost still stay in the linear viscoelastic region. This is a surprising characteristic of the cement paste at micrometre length scale. The validation of linear superposition principle could be of considerable

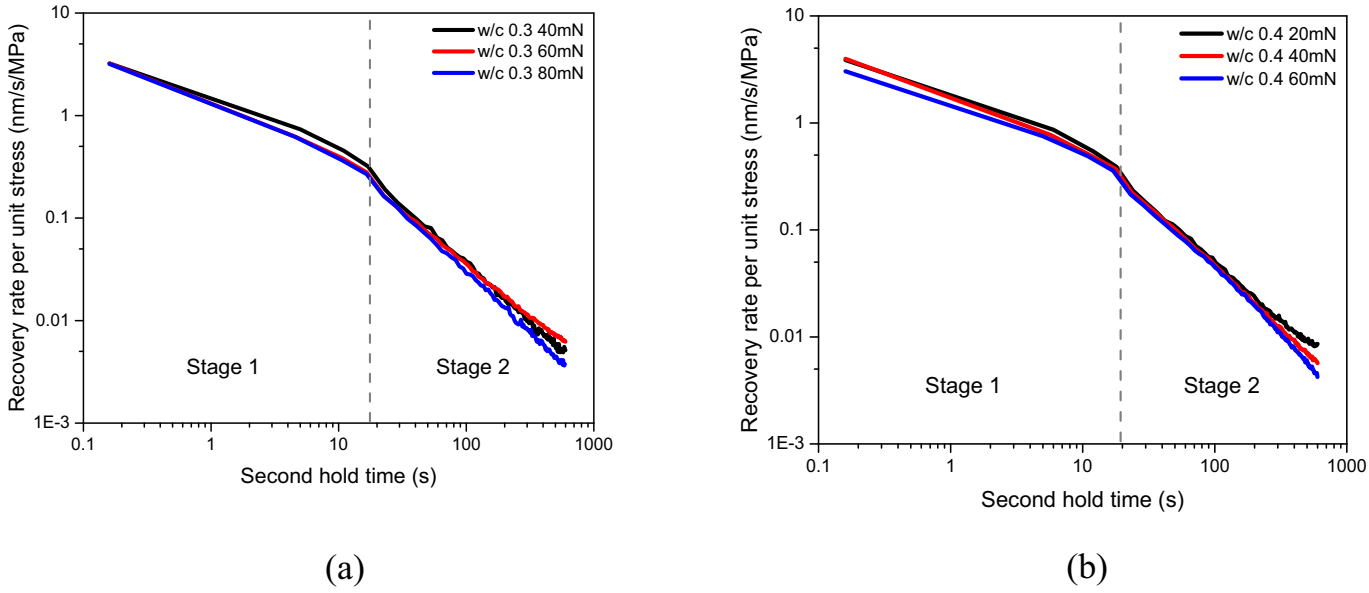

Fig. 16. The measured evolutions of recovery rate per unit stress for different w/c ratios.

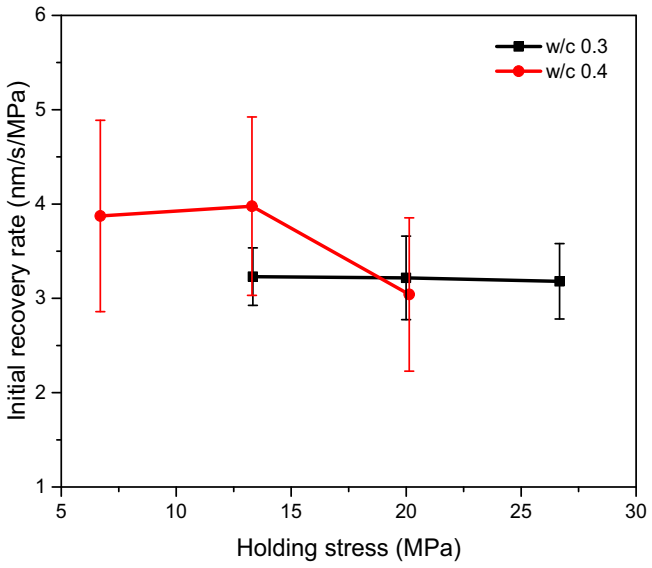

Fig. 17. The calculated initial recovery ratio for different stress levels.

practical relevance in simplifying the calculation of strain under a varying stress and also in providing the basis for creep modelling [33,53,54]. A few creep compliance evolution curves for a constant stress applied to cement paste at different ages may provide adequate information. Theoretical predictions of creep and creep recovery based on BSP have also been studied in macroscopic tests in [33,53]. Moreover, it should be noted that the compressive and tensile creep functions at micrometre length scale are considered to be identical in current study. However, very contradictory findings on the magnitudes of macroscopic compressive creep and tensile creep have been reported in literature [6,55–57], and there is no consensus yet on this issue. Nevertheless, even though the current analytical model is able to accurately predict the time-dependent deformation, there is still a lack of physical explanation with respect to the creep recovery behaviour of cement paste at the microscale. More discussions regarding the creep recovery mechanisms follow in the next sections.

4. Discussion

4.1. Comparisons with microindentation and macroscopic tests

By comparing the test results obtained in this study with the results of conventional microindentation tests and macroscopic tests, it is hoped to gain some insights of the creep recovery behaviour of cement paste at micrometre length scale. Liang and Wei [34] recently investigated the microscopic creep recovery of mature cement paste using microindentation technique. The microindentation creep recovery tests also consist of a minutes-long holding stage and a re-holding stage, which are similar to the loading protocol adopted in this study. The microindentation creep recovery ratio is calculated based on the measured change in indentation depth during the holding stage and the recovery of indentation depth over the re-holding stage. In addition to the similar timeframe, the probed volume in microindentation tests is almost at the same length scale with MCBs. However, the stress magnitude under the indenter tip (Berkovich tip) is one or two orders higher than the stress generated in current bending tests. A distinct quantitative discrepancy can be found in the measured creep recovery ratio. The microindentation recovery ratio for w/c 0.3 cement paste reported in [34] is around 31%–41%, which is much lower than the ratios measured in the current study (>80%). It indicates that most of the measured indentation creep deformations are irrecoverable. Therefore, it can be deduced that different creep mechanisms may be involved in the (almost) fully recoverable power-law function creep obtained in this study and the partially recoverable logarithmic creep measured in indentation tests.

After having initially suggested with Ulm that the logarithmic creep characterized by indentation technique may be related to the rearrangement of nanoscale C-S-H particles [7,28], Vandamme [58] later put forward another possible explanation suggesting that the high stress magnitude under the indenter tip may affect local microscopic relaxations of existing microprestresses or eigenstresses in microstructures, which is also considered as the main long-term creep mechanism in the microprestress-solidification theory [5]. Anyhow, the permanent re-arrangement of C-S-H particles or the local relaxation process may lead to the irreversible creep deformation. Moreover, the recovery ratios obtained in microindentation results seem to be comparable with the long-term macroscopic testing results (21%–33%) reported in [35], where much longer testing durations (>28 days) were used. However, it has to be noted that for conventional macroscopic creep tests on cement

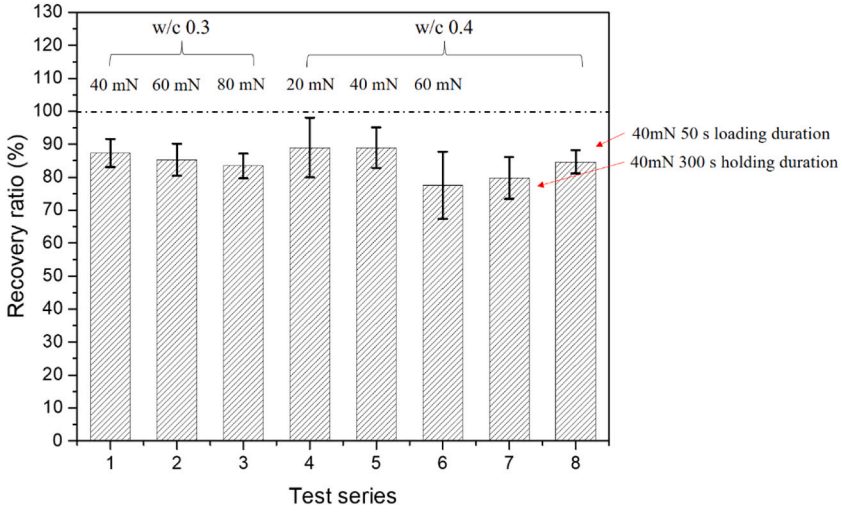

Fig. 18. The calculated recovery ratios for different testing series.

pastes or concretes, the samples would experience significant time-dependent ageing processes, such as ongoing hydration, moisture exchange, microcracking and shrinkage, leading to permanent microstructural changes. As a result, when the external load is removed, these changes could impede the samples to fully return to their original states. This could also explain, to some extent, the irrecoverable creep observed in macroscopic tests.

For the creep recovery of MCB investigated in this study, the governing creep mechanism may not be any of those mechanisms mentioned above as very few irreversible creep deformations were observed. Instead, the testing results are found to be more representative of short-term macroscopic creep recovery results reported in [33], where fully recoverable creep was also observed. In [33], the three-minutes long creep recovery tests on young age cement pastes have been carried out at the macroscale. The identified creep modulus ($1/\alpha$) in [33] is found to increase from 10 to 40 GPa with the increasing hydration degree from approximately 30 to 60%. Note that the reference time used in [33] is 86,400 s. When the same reference time is also used in Eq. (4), the calculated creep modulus for the w/c 0.4 mature cement paste in this study is around 67.7 GPa. Even though the creep modulus may vary with different exponent values, the calculated value is in the same order of magnitude with the results reported in [33]. It is also found in [33] that the power-law exponent (β) decreases slightly from around 0.3 to 0.2 with the increasing hydration degree, which is very close to the exponent obtained in current study (i.e. 0.203). However, it is also interesting to note that in their experiments [33], very low compressive stress level, i.e. 15% of compressive strength (around 3–4 MPa), was used to ensure non-damaging microstructure during the creep tests. By contrast, the flexural stress used in current study amounts to 26 MPa for w/c 0.3 samples (92% of flexural strength), and in this case the cement paste seems to still stay in the linear viscoelastic region. It is worth mentioning that even though only a small part of the beam subjected to the bending load is under this high stress state, the applied stress levels are already much higher than those in macroscopic bending tests. While for w/c 0.4 samples, a relatively lower stress limit, which lies in the range of 13–20 MPa (57–88% of flexural strength), is found to induce non-linear creep. Moreover, it is well known that the flexural and tensile strengths of cementitious materials are almost one order lower than their compressive strengths [59]. In general, a critical maximum value of the stress (or strain) needs to be found to mark the end of the linear viscoelasticity region [60,61]. Beyond this region, the time-dependent responses of materials are different. Knowing this high critical flexural stress for linear viscoelasticity observed at micrometre length scale may be helpful to develop the multiscale modelling of creep of cementitious material in the future.

4.2. *Possible explanations for the observed creep recovery behaviour at micrometre length scale*

In order to further explain the creep recovery behaviour of cement paste at micrometre length scale, several existing mechanisms proposed in literature [3,50,62–64] are discussed and examined in this section.

For any linear viscoelastic material, its time-dependent response can be described using the combinations of elastic spring and viscous dashpot [65]. For instance, when an external tensile load is applied to a Kelvin model, the spring tends to stretch immediately but it will be held back by the dashpot. After the removal of load, the spring starts to return to its initial state and will again be held by the dashpot. As a result, the spring will generate an opposite stress to the dashpot and eventually pull it back to its original position given enough time (for the full recovery). In the case of cement paste at micrometre length scale, one can envision that multiple elastic components, such as unhydrated particles, calcium hydroxide and ettringite, may serve as elastic springs, while only the C-S-H phases may be considered as dashpots [21,66]. The observed creep recovery can be then explained as a microscale stress redistribution process. From this perspective, the non-recoverable creep may be explained by the damaged or changed 'springs' or 'dashpots' potentially due to the microcracking [64]. In addition, Sellevold and Richards [50] also suggested that the short-term creep and creep recovery behaviours of cement paste may be explained as the redistribution of capillary water caused by small stress-induced changes in pore geometry. However, in consideration of the RH (34%) used in this study, the MCB reached the hygral equilibrium before the tests due to its extreme small size and very little free water remained in the capillary pores [22]. Therefore, the explanation based on the redistribution of capillary water is not convincing in the current study. Moreover, due to the low RH some C-S-H phases may be too dry to flow and may also act like non-creep phases to restrain the creep deformation. They could also contribute to the creep recovery in a similar way as other elastic components. Therefore, different time-dependent deformation behaviours may be involved in various RH levels.

In literature, several studies also attempted to explain the creep recovery phenomenon at the C-S-H level. Neville [3] suggested that the creep may be related to the movement of water from the C-S-H gel into the capillary pores, while the creep recovery may be due to the inward movement of water into the gel. In this sense, the creep recovery is explained as a process for cement paste returning to a hygral equilibrium with the ambient medium. Similarly, Meyers and Slate [62] also

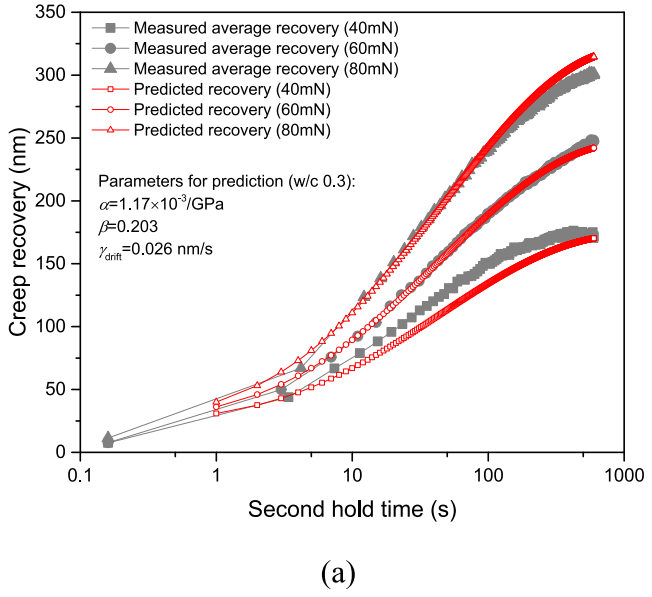

(a)

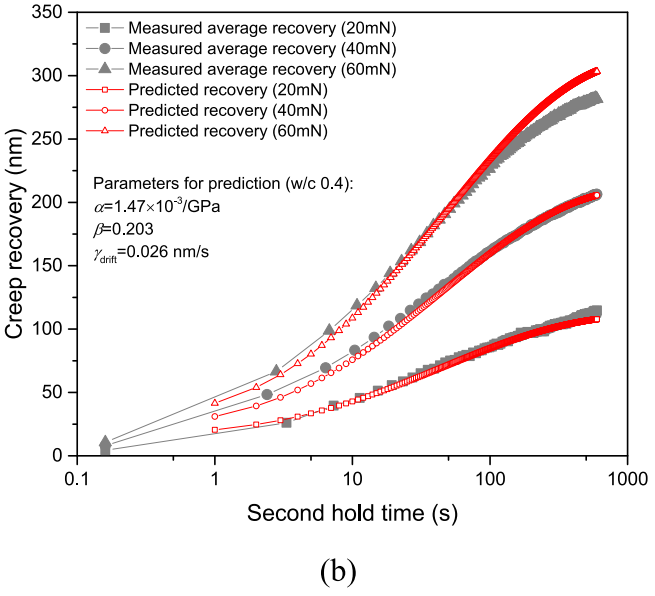

(b)

Fig. 19. The comparisons between the measured and predicted creep recovery curves at the holding stage.

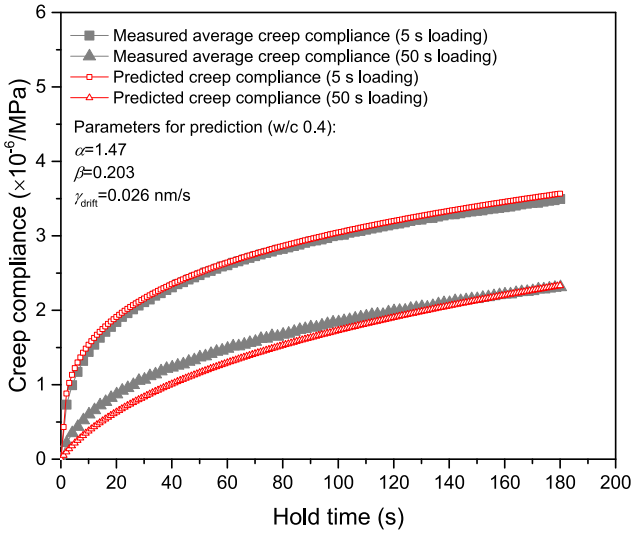

(a)

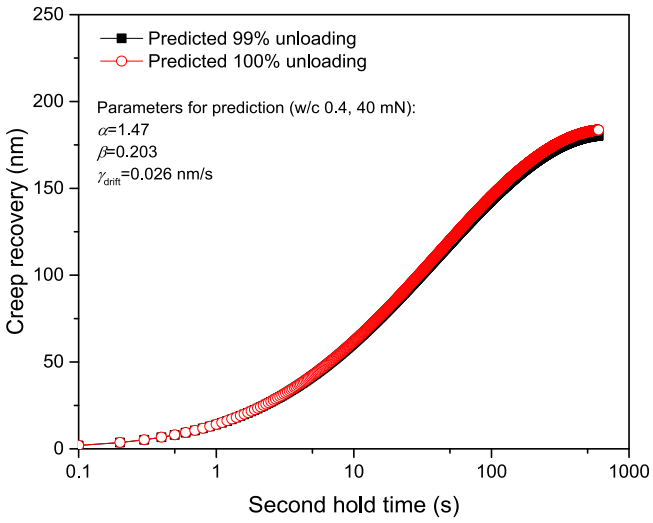

(b)

Fig. 20. (a) The comparison between measured and predicted curves for different loading durations and (b) the effect of different unloading procedure on the predicted creep recovery curves.

suggested that the internal displacement of adsorbed water is recoverable because of the strong attraction of water molecules by closely adjacent gel surfaces. As the gel surfaces are unloaded, water in larger pores will move slowly back towards the attractive gel surfaces. The authors also believe that the physical changes (e.g. ongoing hydration) that take place in the gel during the creep tests could possibly explain the observed irreversible creep. At high relative humidity, Wyrzykowski and Lura [67] showed experimentally that a mechanical load can induce water redistribution in a partially saturated mortar. Furthermore, Wyrzykowski et al. [63] recently using ^{1}H nuclear magnetic resonance (NMR) technique confirmed the fully reversible microdiffusion of water between gel pores and larger pores. The authors also suggested that the partially reversible behaviour could be due to a permanent rearrangement of porosity under load. The hypothesis of water migration (microdiffusion) supported by the NMR results could also explain the short-term creep of MCBs in this study. However, the water transfer may only occur between the small gel pores and large gel pores or interhydrate pores [63] due to the low RH used in this study.

As for the observations regarding the non-linear creep of w/c 0.4 samples under the highest stress level, a possible explanation based on the study of Rossi et al. [64] could be used. In their study [64], the acoustic emission technique was adopted to investigate the macroscopic compressive and tensile creep behaviours of concretes. The authors suggested that during the initial loading stage, microcracking will always occur and the creations of microcracks will generate brutal hygral imbalances within the sample [64]. This will result in the moisture gradients and consequently these gradients will induce water movement from the capillary or gel pores surrounding the microcracks towards these microcracks. This self-drying induced by cracking will cause an additional shrinkage and eventually cause more microcracking due to the restraints of other non-shrinking components. Note that the microcracks induced self-drying shrinkage is assumed to be significant only when the applied stress is high. Therefore, the non-linear creep of w/c 0.4 samples under high stress levels could be explained as the possible appearances of higher density of microcracks. In addition to the

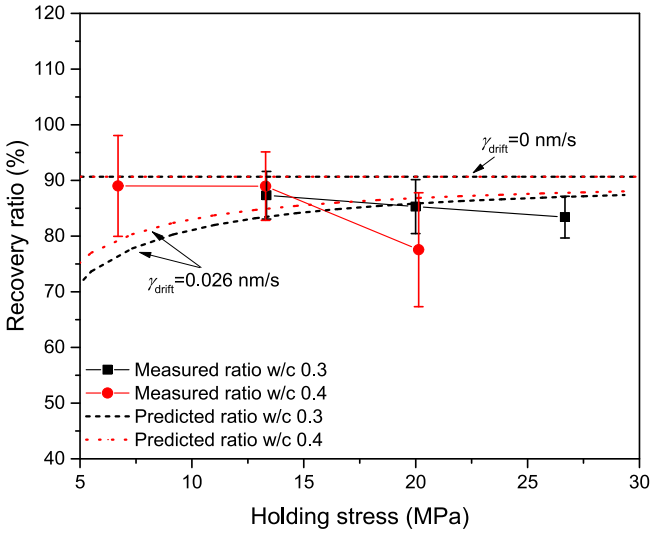

Fig. 21. The comparisons between measured and predicted recovery ratios.

irrecoverable creep deformation caused by microcracking, it can be assumed that a small part of irrecoverable deformation associated with moisture lost to the surroundings is also possible [62] as the samples were not completely sealed, even though the samples were equilibrated before the tests and the overall humidity is kept almost constant in the nanoindenter chamber.

5. Conclusions

This paper studied the creep recovery behaviour of cement paste at micrometre length scale using MCB bending tests. The effects of w/c ratio, flexural stress level and loading history on the creep recovery were investigated. Another purpose of the current paper is to examine whether the linear superposition principle can be employed in the flexural creep and creep recovery of cement paste at micrometre length scale. The following conclusions were drawn from the study:

(1) The MCB bending testing approach, which consists of a holding and a re-holding stage, is useful to characterize the short-term creep recovery of cement paste at micrometre length scale. Compared to recovery ratios obtained in short-term micro-indentation tests and long-term macroscopic tests, much higher recovery ratios (>80%) were obtained in this study.
(2) The analytical model based on the linear superposition principle is able to appropriately predict the time-dependent responses of cement pastes at micrometre length scale, even subjected to very high flexural stress levels (up to 92% of flexural strength for w/c 0.3 samples). Knowing this high flexural stress level applicable for linear viscoelasticity observed at micrometre length scale may be helpful to develop the multiscale modelling of creep of cementitious material in terms of identifications of transitions from linear creep to non-linear creep at different scales.
(3) Several existing short-term creep mechanisms were used to explain the creep and creep recovery behaviour of cement paste at micrometre length scale. It is suggested that the short-term creep recovery may be mainly related to the microscopic stress redistribution process. The possible reversible internal water movement could also be used to explain the creep recovery phenomena. The observed non-linear creep could be attributed to the high density of microcracks promoting the water transfer.

CRediT authorship contribution statement

Yidong Gan: Conceptualization, Methodology, Validation, Formal analysis, Investigation, Writing – original draft. **Matthieu Vandamme:** Conceptualization, Resources, Writing – review & editing, Supervision. **Yu Chen:** Writing – review & editing, Visualization. **Erik Schlangen:** Conceptualization, Resources, Writing – review & editing, Supervision. **Klaas van Breugel:** Conceptualization, Resources, Writing – review & editing, Supervision. **Branko Šavija:** Conceptualization, Resources, Writing – review & editing, Supervision.

Declaration of competing interest

The authors declare no conflict of interest.

Acknowledgement

Yidong Gan and Yu Chen would like to acknowledge the funding supported by China Scholarship Council under grant number 201706130140 and 201807720005, respectively. Mr. Arjan Thijssen is also gratefully acknowledged for his help with the ESEM experiments.

References

[1] C. Stress, B.D. Hannant, Creep and creep recovery of concrete subjected to multiaxial compressive stress, ACI J. Proc. 66 (1969).
[2] A. Ghali, A.M. Neville, P.C. Jha, Effect of elastic and creep recoveries of concrete on loss of prestresss, J. Proc. (1967) 802–810.
[3] A.M. Neville, Recovery of creep and observations on the mechanism of creep of concrete, Appl. Sci. Res. 9 (1960) 71–84.
[4] L.L. Yue, L. Taerwe, Creep recovery of plain concrete and its mathematical modelling, Mag. Concr. Res. 44 (1992) 281–290.
[5] Z.P. Bažant, A.B. Hauggaard, S. Baweja, F.J. Ulm, Microprestress-solidification theory for concrete creep. I: aging and drying effects, J. Eng. Mech. 123 (1997) 1188–1194.
[6] P. Rossi, J.L. Tailhan, F. Le Maou, Comparison of concrete creep in tension and in compression: influence of concrete age at loading and drying conditions, Cem. Concr. Res. 51 (2013) 78–84.
[7] M. Vandamme, F.J. Ulm, Nanogranular origin of concrete creep, Proc. Natl. Acad. Sci. U. S. A. 106 (2009) 10552–10557.
[8] H.M. Jennings, Colloid model of C-S-H and implications to the problem of creep and shrinkage, Mater. Struct. Constr. 37 (2004) 59–70.
[9] O. Bernard, F.J. Ulm, J.T. Germaine, Volume and deviator creep of calcium-leached cement-based materials, Cem. Concr. Res. 33 (2003) 1127–1136.
[10] B.T. Tamtsia, J.J. Beaudoin, Basic creep of hardened cement paste. A re-examination of the role of water, Cem. Concr. Res. 30 (2000) 1465–1475.
[11] H. Ye, Creep mechanisms of calcium–silicate–hydrate: an overview of recent advances and challenges, Int. J. Concr. Struct. Mater. 9 (2015) 453–462.
[12] M. Wyrzykowski, K. Scrivener, P. Lura, Basic creep of cement paste at early age - the role of cement hydration, Cem. Concr. Res. 116 (2019) 191–201.
[14] I. Pignatelli, A. Kumar, R. Alizadeh, Y. Le Pape, M. Bauchy, G. Sant, A dissolution-precipitation mechanism is at the origin of concrete creep in moist environments, J. Chem. Phys. 145 (2016).
[15] P. Havlásek, M. Jirásek, Multiscale modeling of drying shrinkage and creep of concrete, Cem. Concr. Res. 85 (2016) 55–74.
[16] C. Pichler, R. Lackner, Identification of logarithmic-type creep of calcium-silicate-hydrates by means of nanoindentation, Strain. 45 (2009) 17–25.
[17] M. Königsberger, M. Irfan-ul-Hassan, B. Pichler, C. Hellmich, Downscaling based identification of nonaging power-law creep of cement hydrates, J. Eng. Mech. 142 (2016) 1–11.
[18] T. Honorio, B. Bary, F. Benboudjema, Multiscale estimation of ageing viscoelastic properties of cement-based materials: a combined analytical and numerical approach to estimate the behaviour at early age, Cem. Concr. Res. 85 (2016) 137–155.
[19] A.A. Al-Manaseer, M.A. Chiorino, M.A. Issa, K.A. Rieder, Z.P. Bazant, M.A. Daye, H. Marzouk, I. Robertson, J.J. Brooks, W.H. Dilger, Report on factors affecting shrinkage and creep of hardened concrete, Concr. Int. 21 (2005).
[20] R. Alizadeh, J.J. Beaudoin, L. Raki, Viscoelastic nature of calcium silicate hydrate, Cem. Concr. Compos. 32 (2010) 369–376.
[21] A.B. Giorla, C.F. Dunant, Microstructural effects in the simulation of creep of concrete, Cem. Concr. Res. 105 (2018) 44–53.
[22] Y. Gan, M. Vandamme, H. Zhang, Y. Chen, E. Schlangen, K. van Breugel, B. Šavija, Micro-cantilever testing on the short-term creep behaviour of cement paste at micro-scale, Cem. Concr. Res. 134 (2020) 1–26.
[23] Z. Hu, A. Hilaire, J. Ston, M. Wyrzykowski, P. Lura, K. Scrivener, Intrinsic viscoelasticity of C-S-H assessed from basic creep of cement pastes, Cem. Concr. Res. 121 (2019) 11–20.

[24] P. Suwanmaneechot, A. Aili, I. Maruyama, Creep behavior of C-S-H under different drying relative humidities: interpretation of microindentation tests and sorption measurements by multi-scale analysis, Cem. Concr. Res. 132 (2020), 106036.
[25] Q. Zhang, R. Le Roy, M. Vandamme, B. Zuber, Long-term creep properties of cementitious materials: comparing microindentation testing with macroscopic uniaxial compressive testing, Cem. Concr. Res. 58 (2014) 89–98.
[26] H. Zhang, Y. Gan, Y. Xu, S. Zhang, E. Schlangen, B. Šavija, Experimentally informed fracture modelling of interfacial transition zone at micro-scale, Cem. Concr. Compos. 104 (2019).
[27] Y. Wei, S. Liang, X. Gao, Indentation creep of cementitious materials: experimental investigation from nano to micro length scales, Constr. Build. Mater. 143 (2017) 222–233.
[28] M. Vandamme, F.J. Ulm, Nanoindentation investigation of creep properties of calcium silicate hydrates, Cem. Concr. Res. 52 (2013) 38–52.
[29] D.T. Nguyen, R. Alizadeh, J.J. Beaudoin, P. Pourbeik, L. Raki, Microindentation creep of monophasic calcium-silicate-hydrates, Cem. Concr. Compos. 48 (2014) 118–126.
[30] J. Frech-Baronet, L. Sorelli, J.P. Charron, New evidences on the effect of the internal relative humidity on the creep and relaxation behaviour of a cement paste by micro-indentation techniques, Cem. Concr. Res. 91 (2017) 39–51.
[31] S. Mallick, M.B. Anoop, K. Balaji Rao, Early age creep of cement paste - governing mechanisms and role of water-a microindentation study, Cem. Concr. Res. 116 (2019) 284–298.
[32] Y. Gan, H. Zhang, B. Šavija, E. Schlangen, K. van Breugel, Static and fatigue tests on cementitious cantilever beams using nanoindenter, Micromachines. 9 (2018).
[33] M. Irfan-Ul-Hassan, B. Pichler, R. Reihsner, C. Hellmich, Elastic and creep properties of young cement paste, as determined from hourly repeated minute-long quasi-static tests, Cem. Concr. Res. 82 (2016) 36–49.
[34] S. Liang, Y. Wei, New insights into creep and creep recovery of hardened cement paste at micro scale, Constr. Build. Mater. 248 (2020), 118724.
[35] A.M. Neville, Creep of Plain and Structural Concrete, 1983, p. 361.
[36] J. Zhang, G.W. Scherer, Comparison of methods for arresting hydration of cement, Cem. Concr. Res. 41 (2011) 1024–1036.
[37] H. Zhang, B. Šavija, S.C. Figueiredo, M. Lukovic, E. Schlangen, Microscale testing and modelling of cement paste as basis for multi-scale modelling, Materials (Basel) 9 (2016).
[38] Y. Guang, Experimental Study and Numerical Simulation of the Development of the Microstructure and Permeability of Cementitious Materials, 2003.
[39] R.A. Cook, K.C. Hover, Mercury porosimetry of hardened cement pastes, Cem. Concr. Res. 29 (1999) 933–943.
[40] Y. Gan, C.R. Rodriguez, E. Schlangen, K. van Breugel, B. Šavija, Assessing strain rate sensitivity of cement paste at the micro-scale through micro-cantilever testing, Cem. Concr. Compos. 121 (2021).
[41] Y. Gan, C.R. Rodriguez, H. Zhang, Modeling of microstructural effects on the creep of hardened cement paste using an experimentally informed lattice model, Comput. Civ. Infrastruct. Eng. (2021) 1–17.
[42] H. Zhang, Y. Xu, Y. Gan, Z. Chang, E. Schlangen, B. Šavija, Microstructure informed micromechanical modelling of hydrated cement paste: techniques and challenges, Constr. Build. Mater. 251 (2020), 118983.
[43] H. Zhang, B. Šavija, Y. Xu, E. Schlangen, Size effect on splitting strength of hardened cement paste: experimental and numerical study, Cem. Concr. Compos. 94 (2018) 264–276.
[44] H. Zhang, B. Šavija, S.C. Figueiredo, E. Schlangen, Experimentally validated multi-scale modelling scheme of deformation and fracture of cement paste, Cem. Concr. Res. 102 (2017) 175–186.
[45] W.C. Oliver, G.M. Pharr, An improved technique for determining hardness and elastic modulus using load and displacement sensing indentation experiments, J. Mater. Res. 7 (1992) 1564–1583.
[46] W. Cooke, P. Howell, Viscoelastic behaviour of glass and “fictive temperature”, Math. Ind. 372 (1998) 22.
[47] M.E. Gurtin, E. Sternberg, On the linear theory of viscoelasticity, Arch. Ration. Mech. Anal. 7 (1961) 402–411.
[48] K. Van Breugel, Relaxation of Young Concrete, 1980, p. 144.
[49] M. Ausweger, E. Binder, O. Lahayne, R. Reihsner, G. Maier, M. Peyerl, B. Pichler, Early-age evolution of strength, stiffness, and non-aging creep of concretes: experimental characterization and correlation analysis, Materials (Basel) 12 (2019) 207.
[50] E.J. Sellevold, C.W. Richards, Short-time creep transition for hardened cement paste, J. Am. Ceram. Soc. 55 (1972) 284–289.
[51] S. Liang, Y. Wei, Effects of water-to-cement ratio and curing age on microscopic creep and creep recovery of hardened cement pastes by microindentation, Cem. Concr. Compos. 113 (2020), 103619.
[52] J.M. Illston, The components of strain in concrete under sustained compressive stress, Mag. Concr. Res. 17 (1965) 21–28.
[53] Y. Huang, L. Xiao, J. Gao, Y. Liu, Tensile creep and unloading creep recovery testing of dam concrete with fly ash, J. Mater. Civ. Eng. 31 (2019).
[54] Z.P. Bažant, Numerical determination of long-range stress history from strain history in concrete, Mater. Constr. 5 (1972) 135–141.
[55] J.P. Forth, Predicting the tensile creep of concrete, Cem. Concr. Compos. 55 (2015) 70–80.
[56] S. Liang, Y. Wei, Methodology of obtaining intrinsic creep property of concrete by flexural deflection test, Cem. Concr. Compos. 97 (2019) 288–299.
[57] N. Ranaivomanana, S. Multon, A. Turatsinze, Tensile, compressive and flexural basic creep of concrete at different stress levels, Cem. Concr. Res. 52 (2013) 1–10.
[58] M. Vandamme, Two models based on local microscopic relaxations to explain long-term basic creep of concrete, Proc. R. Soc. A 474 (2018), 20180477.
[59] H. Zhang, Y. Xu, Y. Gan, Z. Chang, E. Schlangen, B. Šavija, Combined experimental and numerical study of uniaxial compression failure of hardened cement paste at micrometre length scale, Cem. Concr. Res. 126 (2019).
[60] Z. Sun, T. Voigt, S.P. Shah, Rheometric and ultrasonic investigations of viscoelastic properties of fresh Portland cement pastes, Cem. Concr. Res. 36 (2006) 278–287.
[61] S.M. Mansour, M.T. Abadlia, K. Bekkour, I. Messaoudene, Improvement of rheological behaviour of cement pastes by incorporating metakaolin, Eur. J. Sci. Res. 42 (2010) 442–452.
[62] B.L. Meyers, F.O. Slate, Creep and creep recovery of plain concrete as influenced by moisture conditions and associated variables, Mag. Concr. Res. 22 (1970) 37–41.
[63] M. Wyrzykowski, A.M. Gajewicz-Jaromin, P.J. McDonald, D.J. Dunstan, K. L. Scrivener, P. Lura, Water redistribution-microdiffusion in cement paste under mechanical loading evidenced by 1H NMR, J. Phys. Chem. C 123 (2019) 16153–16163.
[64] P. Rossi, J.L. Tailhan, F. Le Maou, L. Gaillet, E. Martin, Basic creep behavior of concretes investigation of the physical mechanisms by using acoustic emission, Cem. Concr. Res. 42 (2012) 61–73.
[65] Z.P. Bazant, S.T. Wu, Dirichlet series creep function for aging concrete, ASCE J. Eng. Mech. Div. 99 (1973) 367–387.
[66] V. Šmilauer, Z.P. Bažant, Identification of viscoelastic C-S-H behavior in mature cement paste by FFT-based homogenization method, Cem. Concr. Res. 40 (2010) 197–207.
[67] M. Wyrzykowski, P. Lura, The effect of external load on internal relative humidity in concrete, Cem. Concr. Res. 65 (2014) 58–63.
[68] Y. Gan, H. Zhang, Y. Zhang, Y. Xu, E. Schlangen, K. van Breugel, B. Šavija, Experimental study of flexural fatigue behaviour of cement paste at the microscale, Int. J. Fatigue. 151 (2021).